Rigid-band electronic structure of scandium nitride across the *n*-type to *p*-type carrier transition regime

Sanjay Nayak,[1,2] Madhusmita Baral,[3,4] Mukul Gupta,[5] Jaspreet Singh,[6] Magnus Garbrecht,[7] Tapas Ganguli,[3,4] S. M. Shivaprasad,[1,2] and Bivas Saha[1,2,8,*]

[1]*Chemistry and Physics of Materials Unit, Jawaharlal Nehru Centre for Advanced Scientific Research, Bangalore 560064, India*
[2]*International Centre for Materials Science, Jawaharlal Nehru Centre for Advanced Scientific Research, Bangalore 560064, India*
[3]*Raja Ramanna Centre for Advanced Technology, Indore 452013, India*
[4]*Homi Bhabha National Institute, Training school complex, Anushakti Nagar, Mumbai 400094*
[5]*UGC-DAE Consortium for Scientific Research, Khandwa Road, Indore-452017, India*
[6]*Technical Physics Division, Bhabha atomic research Centre, Mumbai 400094*
[7]*Australian Centre for Microscopy and Microanalysis, The University of Sydney, NSW 2006, Australia*
[8]*School of Advanced Materials (SAMat), Jawaharlal Nehru Centre for Advanced Scientific Research, Bangalore 560064, India*

Intentional doping and unintentional impurities in intrinsic semiconductors generate carriers that enable device operations. Fundamental to the electronic activity of dopants and impurities is the introduction of defect states inside the forbidden energy gap of semiconductors having shallow and/or deep characteristics, which fundamentally define the ability to engineer its physical properties and associated device performance. Here we demonstrate that unintentional electron doping by oxygen (O_N) impurities and intentional magnesium hole doping (Mg_{Sc}) in scandium nitride (ScN) do not introduce any defect states inside its fundamental bandgap and that the rigid-band electronic structure remains unchanged. Employing a combination of spectroscopic techniques as well as first-principles density functional theory analysis, we show that the O_N and Mg_{Sc} defect states in ScN are located inside the bands, which leaves behind the virgin ScN bandgap as well as the valence and conduction band edges that are important for electronic transport. The rigid-band electronic structure of ScN with respect to the electron and hole doping results in high electron and hole concentrations due to the free movement of Fermi level and results in tunable electronic and thermoelectric properties necessary for device applications.

Nanoscale control of defects in semiconducting materials is crucial for engineering its structural, electronic, and opto-electronic properties [1,2]. Point defects such as vacancies, interstitials, foreign impurities, etc., and line defects such as dislocations, grain boundaries, etc., significantly impact the physical properties of an otherwise perfect semiconductor [3–5]. Electronically active point defects such as intentional doping of *n*-type (electron) and *p*-type (hole) carriers as well as native defects such as vacancies and impurities introduce defect states inside the bandgap of a semiconductor with shallow and/or deep characteristics [6,7]. For example, in technologically important III-nitride semiconductors such as GaN, a combination of experimental and modeling analysis have demonstrated that *p*-type doping by Mg_{Ga} incorporation introduces shallow acceptor states at ~200 meV from the valence band edge [8–10], while recent theoretical reports have suggested deep defect states at ~600 meV [11]. In InN, experimental analysis has shown that Mg (hole) doping introduces shallow acceptor states ~110 meV from the valence band edge [12]. Similar to the hole doping, incorporation

of *n*-type foreign impurities such as oxygen (O_N) and N vacancies (V_N) introduce shallow donor states close to the conduction band (CB) edge in GaN [13,14]. Apart from III-nitrides, electronically active defects in practically all classes of semiconducting materials exhibit states inside the bandgap, with examples of III-arsenides like GaAs [15], InAs [16]; III-phosphides like InP [17], GaP [18]; III-antimonides such as GaSb [19], AlSb [20]; and other II-IV semiconductors such as CdTe [21,22], ZnSe [23], etc.

While defect states inside the bandgap provide carriers, such electronic states may also act as nonradiative recombination centers that quench luminescence [24,25], reduce carrier mobility [26], and pin the Fermi level [27] affecting device performance. For example, Mg dopant states in GaN, located ~0.2 eV above the valence band maxima (VBM) demand high activation energy [28], which limits the ability to synthesize heavily *p*-doped GaN [29]. Therefore, the most desired case for the electronic activity of the defects would be to dope a semiconductor with high *n*-type and *p*-type carriers, without the creation of defect states inside its bandgap. This would lead to desired electron and hole concentrations, without the necessity to deal with the defect states and its potentially adverse impacts, thus leading to efficient electronic, thermo-electric, light emitting, and transistor devices.

---

*Author to whom correspondence should be addressed: bsaha@jncasr.ac.in; bivas.mat@gmail.com

Scandium nitride (ScN) is a group III (B)-nitride indirect bandgap semiconductor that crystallizes in rocksalt structure having octahedral bonding coordination, and has attracted significant interest in recent years for its thermoelectric applications [30,31], as a substrate to deposit high quality GaN with reduced dislocations [32] and as a semiconductor component for epitaxial metal/semiconductor superlattice metamaterial development [33,34]. Due to the presence of unwanted oxygen impurities, as-deposited ScN thin films are *n*-type degenerate semiconductors [35,36] with carrier concentrations in the range of $(2-4) \times 10^{20}$ cm^{-3}. Mg doping has proven to be effective in reducing the *n*-type carrier concentrations in ScN [37] leading to an *n*-to-*p* carrier-type transition with high hole concentrations $(2.2 \times 10^{20}$ cm$^{-3})$, leading to the presumption that self-compensation effects are perhaps not significant in ScN [see Sec. II of the Supplemental Material (SI) [38] for a detailed discussion].

Previous theoretical calculation [35] based on a Heyd-Scuseria-Ernzerhof (HSE) functional on ScN and Sc$_{1-x}$Mg$_x$N have shown no thermodynamically stable charged transition levels in the bandgap with an energetically favorable defect(s). Optical absorption measurements also showed no sign of any subbandgap absorption [37], hinting an absence of defect states in the bandgap. In this paper, we demonstrate that although the incorporation of unwanted O$_N$ impurities leads to a high electron concentration of $\sim(2-4) \times 10^{20}$ cm^{-3}, and intentional Mg$_{Sc}$ (hole) doping results in a high hole concentration of $\sim 2 \times 10^{20}$ cm^{-3} in sputter deposited ScN thin films, the rigid-band electronic structure remains unchanged with respect to the introduction of defects. In other words, Mg$_{Sc}$ and O$_N$ do not introduce any acceptor or donor defect states inside ScN's bandgap respectively, and the band edge properties that determine electronic transport remain unchanged.

First-principles density functional theory (DFT) calculations were carried out using plane wave basis code QUANTUM ESPRESSO [39–43] within DFT+U formalism [details in Sec. I(C) of the SI [38]]. For pure ScN, the valence band is primarily composed of N-*2p* orbitals with contributions from Sc 3*d*-*e$_g$* states, while the conduction band exhibits Sc 3*d*-*t$_{2g}$* characteristics with a small contribution from N-*2p* orbitals [see Fig. 1(a)]. Unlike other wurtzite III-nitride semiconductors, the *p-d* hybridization in ScN is responsible for the bandgap opening, as it splits the Sc-*3d* orbitals similar to the case of FeGa$_3$ and RuGa$_3$ [44]. With the incorporation of oxygen (O$_N$) of $\sim 3.1\%$ (ScN$_{0.969}$O$_{0.031}$), the Fermi level moves inside the conduction band, ~ 0.37 eV from the band edge. As oxygen atom contains one extra electron compared to nitrogen, it acts as a donor in ScN. Densities of states (DOS) calculations [see Figs. 1(b) and 1(d)] show that the O 2*p* states are in resonance with N 2*p* orbitals and are located deep inside the valence band with a peak at ~ -5 eV and small densities at ~ -2.5 eV from the valence band edge. The densities of O 2*p* states in the conduction band were minimal, though in resonance with Sc-*d* states. Since electronic transport is primarily determined by states that are close to the Fermi level, i.e., states inside the bandgap and a narrow region of the band edges for a semiconductor; for all practical purposes, the oxygen impurity (O$_N$) states would not affect transport properties except for donating carriers, which manifests itself in the heavy *n*-type carrier concentrations in
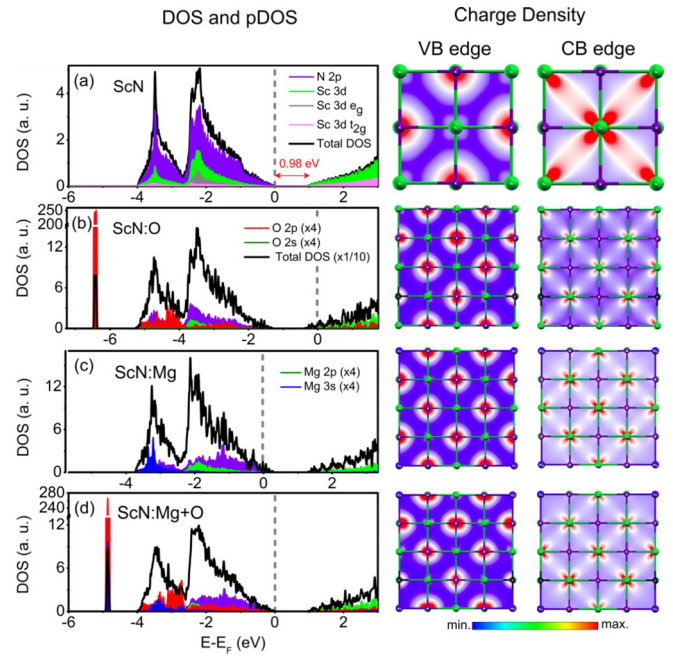

FIG. 1. Total and partial density of electronic states of ScN with various defects configurations. Fermi level is set as 0 eV. The charge densities of VBM-100 meV and conduction band maxima (CBM)+100 meV are shown at the right side of the each DOS plot.

as-deposited ScN films. Similarly, though the incorporation of Mg inside ScN (Mg$_{Sc}$) shifts the Fermi level inside the valence band at ~ 0.32 eV from the band edges for 3.1% Mg doped in ScN (Sc$_{0.969}$Mg$_{0.031}$N) due to carrier compensation effects [see Figs. 1(c) and 1(d)], the Mg 2*p* and 3*s* states are located deep inside the bands around ~ -2.5 to -3.5 eV and -2.7 to -4.0 eV from the valence band edges, respectively. The Mg states are also in resonance with the N 2*p* states and thus should not affect transport properties, except for hole generation.

However, first-principles analysis showed that the presence of V$_N$ would add defect states close to the valence band edge and significantly alter the rigid band electronic structure [45]. A distinct peak having Sc 3*d*-*e$_g$* characteristics (details in Sec. V of the SI [38]) emerged for ScN having 3.1% of V$_N$. The presence of the vacancy pushed the Fermi level inside the conduction band that represents its donor characteristics. Without the ionic relaxation that minimizes forces on atoms around the vacancy, the defect state was found to occupy the top of the valence band edge. When full ionic relaxation steps were performed, the defect state was found to be localized inside the bandgap at ~ 0.06 eV from the valence band edges and has a dispersion width of 0.43 eV. Calculated defect formation energies (FE) suggest that both the V$_N$ and O$_N$ are energetically favorable for Sc-rich ScN growth conditions [35]. Theoretical analysis has also suggested that O$_N$ exhibits lower FE compared to V$_N$ under Sc-rich conditions, while under N-rich growth conditions, the FE of V$_N$ is very high [35]. Nevertheless, it must be emphasized that for electronic and optoelectronic device applications, ScN thin films should be deposited in N-rich conditions to minimize the V$_N$ concentrations.

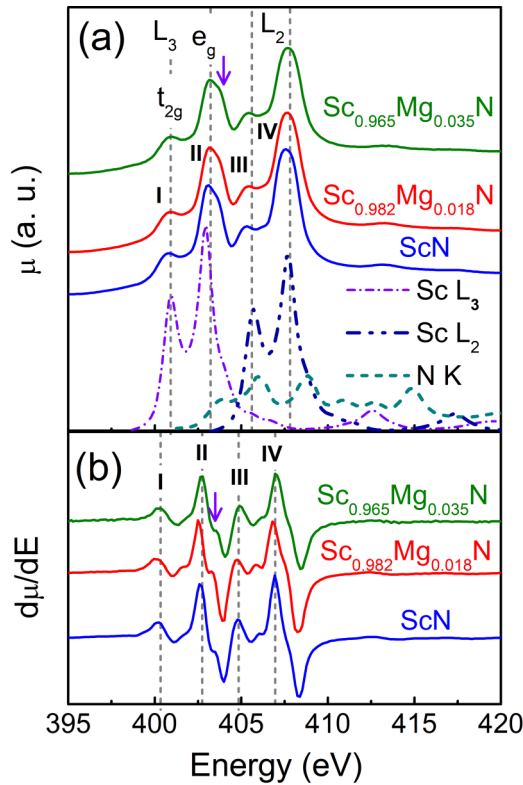FIG. 2. (a) SXAS data of ScN and $Sc_{1-x}Mg_xN$ thin films and (b) their first derivatives represents the absorption edges. Dotted lines in (a) are theoretically calculated ones for pure ScN configuration.

First-principles analysis was also utilized to determine the possible clustering of atoms inside ScN, as such clusters are known to significantly impact the performance of materials. Previous [31] and current theoretical analysis on oxygen doped ScN have shown no O-O or Mg-Mg clustering tendency in ScN, which is consistent with experimental results (see Fig. S3 of the SI [38]). Results also showed that for Mg_{Sc}-O_N (near) (separation between Mg_{Sc} and $O_N(d) \approx 2.30$ Å) is energetically preferable by 50 meV/8 atom unit cells in comparison to Mg_{Sc}-O_N (far) ($d \approx 6.90$ Å).

For the experimental validation of electronic structure calculations, ScN and $Sc_{1-x}Mg_xN$ thin films were deposited on (001) MgO substrates in N-rich growth conditions with high vacuum dc-sputtering method. As-deposited ScN thin film was degenerately n-doped due to the presence of oxygen impurities (details in Secs. II and IV(B) and IV(C) of the SI [38]) [37]. For the spectroscopic analysis, an undoped n-type ScN thin film having $n_e = 2.9 \times 10^{20}$ cm^{-3} and two p-type samples $Sc_{0.982}Mg_{0.018}N$ and $Sc_{0.965}Mg_{0.035}N$ with hole densities of $n_h = 5.7 \times 10^{19}$ and $n_h = 1.1 \times 10^{20}$ cm^{-3}, respectively, were chosen.

Unoccupied densities of electronic states were measured with soft x-ray absorption spectroscopy (SXAS) measurements [46,47] that reveal four distinct peaks in all three films with very similar spectral shapes. The four peak positions from different films are close to one another and are located at 400.83 eV (I), 403.17 eV (II), 405.43 eV (III), and 407.70 eV (IV), respectively, which lead to similar absorption thresholds [see Fig. 2(a)]. Moreover, a shoulder peak was also found at

403.57 eV [the marked feature in Figs. 2(a) and 2(b)]. Such identical spectral shape and peak positions indicate that Mg doping of n-type ScN does not perturb the band dispersion and the charge introduction remains within the muffin tin radius of Mg ions.

As the Sc L edge and N K edge appear very close to one another, the experimental absorption spectra were compared with spectra obtained from full multiscattering (FMS) theory [44,48], and the peak I and II in Fig. 2(a) are assigned to the L_3 edge of Sc, while peak III and IV are assigned to the L_2 edge. The L_3 edge is the transition from Sc $2p_{3/2}$ to unoccupied d orbitals, whereas, L_2 represents transitions from Sc $2p_{1/2}$ to unoccupied d orbitals. In addition, due to the octahedral symmetry in the crystal structure, both the L_3 and L_2 subbands split into t_{2g} and e_g orbitals, where e_g are located at higher energies than the t_{2g}. The separation between L_3 and L_2 edge [$L_2(t_{2g}) - L_3(t_{2g})$] is ~4.5 eV, which is consistent with other 3d material systems [49]. It is important to note that the splitting due to spin-orbit coupling of the 2p orbital (ζ_{2p}) of the Sc atom obtained from an XPS 2p core level scan is also ~4.5 eV (details in Fig. S6 of the SI [38]), the same as the separation between the L_3 and L_2 edges. The crystal field splitting energy (~10 Dq) estimated from the SXAS [energy difference between the peak of e_g and t_{2g} from Fig. 2(a)] is 2.2 eV, which is close to the estimated value of 2.1 eV obtained with FMS theory [see Fig. 2(a)]. Both 10 Dq and ζ_{2p} of Sc are consistent with previously reported values for $SmScO_3$ and other rare-earth element doped ScO_3 [50,51]. Such similar values of the crystal field splitting parameters of undoped ScN and p-type $Sc_{1-x}Mg_xN$ films demonstrate that there is no effective change in the conduction band structure with O_N and Mg_{Sc} doping, and the defect states related to the dopants appear primarily inside the bands. The SXAS also agreed well with the experimental electron-energy-loss-spectroscopy (EELS) spectra (details in Sec. IV(A) of the SI [38]).

Ultraviolet photoemission (UPS) spectra were obtained (see Fig. 3, SI [38], and Refs. [52–55]) to understand the valence band densities of electronic states (DOS) along with the defect levels, and are compared to the electronic structure calculations. The photoemission spectral shape of all three samples are compared to each other, and a distinct edge in the valence band around −1.0 eV is visible. The valence band on-set values of −1.04, −0.47, and −0.47 eV were obtained for ScN, $Sc_{0.982}Mg_{0.018}N$, and $Sc_{0.965}Mg_{0.035}N$, respectively (see Fig. 3). For undoped ScN, previous [30,37,56] experimental and theoretical analyses have suggested that the Fermi level is situated inside the conduction band at ~0.06−0.2 eV above the band edge that is consistent with our observation. Moreover, the spectra show that with Mg doping, the Fermi level shifts from the conduction band towards the valence band due to carrier compensation effects, which is again consistent with first-principles analysis [see Fig. 1(c)] and transport measurements (later discussed in Fig. 4). It is, however, important to note that though the carrier concentration of $Sc_{0.965}Mg_{0.035}N$ is twice that of $Sc_{0.982}Mg_{0.018}N$, the valence band edges for both of the p-type samples were close to one another due to surface Fermi level pinning of the p-type $Sc_{1-x}Mg_xN$. Though DFT calculations and previous experimental analysis suggest that the Fermi level is expected to be close to or inside the
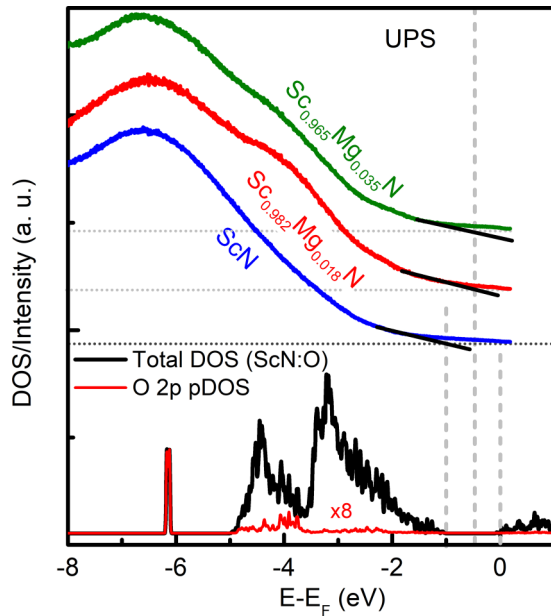
FIG. 3. Valence band spectra of ScN and $Sc_{1-x}Mg_xN$ obtained with UPS measurements are presented. Comparison between theoretically calculated DOS of ScN:O and UPS valence band spectra of ScN is shown. The Fermi level of theoretically calculated DOS was adjusted with the experimental value.

valence band [30] for such *p*-type films, surface Fermi level pinning is not surprising as other III-nitrides [57] such as InN [58] also exhibit similar behavior. In a recent report [36], Mg ion-implantation has been utilized to introduce defects for reducing thermal conductivity in ScN and to explore the potential for achieving *p*-type ScN films. However, since the as-deposited ScN exhibited a large oxygen concentration (~ 9 at. %), no *p*-type conduction was observed even at a maximum 2.2 at. % incorporation of Mg inside ScN.
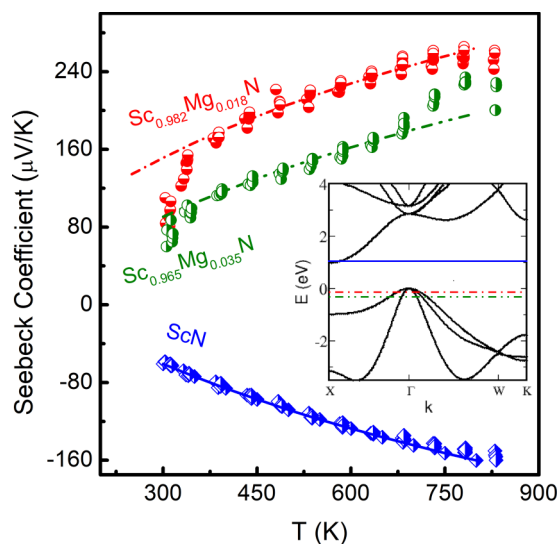

FIG. 4. Temperature dependent Seebeck coefficient of *n*-type ScN and *p*-type $Sc_{1-x}Mg_xN$ thin film alloys are presented. Solid lines represent theoretical data calculated using electronic dispersion of pure ScN (shown on insets with respective Fermi levels).

It may be also noted that there are some differences in the features of the valence band spectra obtained from the UPS measurements and the calculated valence band density of states. To understand these differences, we analyze the XPS Sc $3d$ photoemission data obtained from Al K_α source (1.486 keV) and 4.357-keV x-ray source (details in Sec. IV(C) of the SI [38] and Ref. [59]). Comparison between the two shows that the intensity ratio of the Sc $3d$ peak from the Sc-O and from Sc-N bond is less from the 4.357-keV excitation for Mg-doped samples ($I_{Sc-N} : I_{Sc-O}$ (1.486 keV)$/I_{Sc-N} : I_{Sc-O}$ (4.357 keV) $=$ 0.2317 for $Sc_{0.982}Mg_{0.018}N$ and 0.5334 for $Sc_{0.965}Mg_{0.035}N$ and the value is almost unity in undoped ScN. The escape depth of the core electrons with an excitation of ~ 4 keV is about 5 nm and is less than 2 nm for Al K_α excitation. Hence, it was concluded that there is a larger concentration of oxygen at the surface as compared to the bulk of the ScN films. Since the presence of such oxygen on the sample surface appears primarily from postgrowth exposure to the ambient conditions, they could be present in both scandium oxide (Sc_2O_3) and scandium oxy-nitride (ScO_xN_y) forms. However, a close comparison of XPS core level spectra determined here and its comparison with Ref. [38] suggest that oxygen is present most likely in oxy-nitride from, though the presence of scandium oxide can never be ruled out (see Sec. VII in the SI [38] and Ref. [60] for a detailed discussion).

The peak of the valence band is found at a binding energy of 6.2 eV, which corresponds to the calculated oxygen partial density of states in the valence band (see Fig. 3). The presence of increased oxygen at the surface of the ScN films, coupled with the large photoemission cross section of O $2p$ states at 21.2-eV excitation, contributes to the dominance of the O-related feature and broadening of the valence band states, as observed in the experiments. It may be noted that the observation of the broadening of the valence band due to the presence of oxygen is in spite of the fact that the sample surfaces were cleaned by ion etching (details in Sec. IV(B) of the SI [38] and Ref. [61]). The system base vacuum was $\sim 9 \times 10^{-11}$ mbar and instrument resolution was better than 20 meV. Thus, the observations are intrinsic to ScN surface density of states and not extrinsic surface impurity effects. However, the determination of the valence band onset is unambiguous in spite of this smearing out of the states, because the bandgap of Sc_2O_3 [62] is > 5.6 eV. For scandium oxy-nitride (ScN: Sc_2O_3) the bandgap is expected to be more than 3.25 eV, (whose presence cannot be completely ruled out with an increase in oxygen at the surface), and hence will not affect the ScN valence band onset values [63].

While the spectroscopic characterization and first-principles analysis clearly confirmed the rigid band electronic structure of ScN with respect to the O_N and Mg_{Sc}, its manifestation on the thermoelectric and electronic transport properties are more clear and impacting. The validation of the rigid band electronic structure was further supported by the temperature-dependent Seebeck measurements and theoretical calculations of the Seebeck coefficient with Boltzmann transport theory [64] and Landauer models [31], which use an electronic dispersion spectrum of pure ScN. Both the models have been able to capture increasing Seebeck coefficients as a function of temperature (see Fig. 4) with the

electronic dispersion of pure ScN, and having the Fermi level placed at the appropriate positions in the band structure, and suitable scattering models (shown in Fig. 4). The increase in resistivity of $Sc_xMg_{1-x}N$ films at room temperature with increasing Mg concentrations for the n-type carrier regime and decrease in the p-type region [37] also clearly indicate the absence of any defect states inside the bandgap and the Fermi level moving from the conduction band to the valence band (details in Sec. II of the SI [38]).

In conclusion, spectroscopic and first-principles analysis has demonstrated that the rigid band electronic structure of ScN remain unchanged with respect to the incorporation of oxygen (O_N) that acts as an electron dopant and magnesium (Mg_{Sc}) that acts as a hole dopant, leading to high n-type and p-type carrier concentrations, respectively. Contrary to other wurtzite III-nitride semiconductors, the defects states in ScN are located deep inside the bands and do not introduce any changes to the ScN bandgap and its band edges. Due to the rigid band electronic structure, the Fermi level moves freely from the conduction to valence band and leads to an n-to-p-type carrier transition, with high electron and hole concentrations, and tunable electronic and thermoelectric properties. The rigid-band electronic structure of ScN with respect to the electron and hole doping is quite unique and interesting, not only among the III-V semiconducting materials, but for most well-known semiconductors in general, and is expected to stimulate interest from researchers to harness its potential for device applications.

---

[1] L. Vicarelli, S. J. Heerema, C. Dekker, and H. W. Zandbergen, ACS Nano **9**, 3428 (2015).

[2] J. Narayan, J. Appl. Phys. **100**, 034309 (2006).

[3] R. E. Smallman, *Modern Physical Metallurgy* (Elsevier, Amsterdam, 2016).

[4] M. Li, Y. Wan, L. Tu, Y. Yang, and J. Lou, Nanoscale Res. Lett. **11**, 155 (2016).

[5] M. Jiang, H. Xiao, S. Peng, L. Qiao, G. Yang, Z. Liu, and X. Zu, Nanoscale Res. Lett. **13**, 301 (2018).

[6] H. Kim, J. Lee, S.-J. Kahng, Y.-W. Son, S. B. Lee, C.-K. Lee, J. Ihm, and Y. Kuk, Phys. Rev. Lett. **90**, 216107 (2003).

[7] E. Kucur, W. Bücking, R. Giernoth, and T. Nann, J. Phys. Chem. B **109**, 20355 (2005).

[8] E. Cimpoiasu, E. Stern, R. Klie, R. A. Munden, G. Cheng, and M. A. Reed, Nanotechnology **17**, 5735 (2006).

[9] B. Monemar, S. Khromov, G. Pozina, P. Paskov, P. Bergman, C. Hemmingsson, L. Hultman, H. Amano, V. Avrutin, X. Li, and H. Morkoç, Jpn. J. Appl. Phys. **52**, 08JJ03 (2013).

[10] M. A. Reshchikov and H. Morkoç, J. Appl. Phys. **97**, 061301 (2005).

[11] J. L. Lyons, A. Janotti, and C. G. Van De Walle, Phys. Rev. Lett. **108**, 156403 (2012).

[12] P. A. Anderson, C. H. Swartz, D. Carder, R. J. Reeves, S. M. Durbin, S. Chandril, and T. H. Myers, Appl. Phys. Lett. **89**, 184104 (2006).

[13] S. Nayak, M. H. Naik, M. Jain, U. V. Waghmare, and S. M. Shivaprasad, arXiv:1710.05670.

[14] K. Laaksonen, M. G. Ganchenkova, and R. M. Nieminen, J. Phys.: Condens. Matter **21**, 015803 (2009).

[15] J. S. Kim, I. H. Bae, J. Y. Leem, S. K. Noh, J. I. Lee, J. S. Kim, S. M. Kim, J. S. Son, and M. Jeon, J. Cryst. Growth **226**, 52 (2001).

[16] C. L. Dos Santos, T. M. Schmidt, and P. Piquini, Nanotechnology **22**, 265203 (2011).

[17] M. H. M. Van Weert, O. Wunnicke, A. L. Roest, T. J. Eijkemans, A. Y. Silov, J. E. M. Haverkort, G. W. T Hooft, and E. P. A. M. Bakkers, Appl. Phys. Lett. **88**, 43109 (2006).

[18] D. Olego and M. Cardona, Phys. Rev. B **22**, 886 (1980).

[19] R. D. Wiersma, J. A. H. Stotz, O. J. Pitts, C. X. Wang, M. L. W. Thewalt, and S. P. Watkins, Phys. Rev. B **67**, 165202 (2003).

[20] B. R. Bennett, W. J. Moore, M. J. Yang, and B. V Shanabrook, J. Appl. Phys. **87**, 7876 (2000).

[21] T. Ablekim, S. K. Swain, W.-J. Yin, K. Zaunbrecher, J. Burst, T. M. Barnes, D. Kuciauskas, S.-H. Wei, and K. G. Lynn, Sci. Rep. **7**, 4563 (2017).

[22] S. H. Wei and S. B. Zhang, Phys. Rev. B **66**, 155211 (2002).

[23] I. S. Hauksson, J. Simpson, S. Y. Wang, K. A. Prior, and B. C. Cavenett, Appl. Phys. Lett. **61**, 2208 (1992).

[24] M. A. Reshchikov, D. O. Demchenko, J. D. McNamara, S. Fernández-Garrido, and R. Calarco, Phys. Rev. B **90**, 035207 (2014).

[25] F. Auzel, G. Baldacchini, L. Laversenne, and G. Boulon, Opt. Mater. (Amsterdam, Neth.). **24**, 103 (2003).

[26] M. Aven and B. Segall, Phys. Rev. **130**, 81 (1963).

[27] T. Nishimura, K. Kita, and A. Toriumi, Appl. Phys. Lett. **91**, 123123 (2007).

[28] A. V. Mazalov, D. R. Sabitov, V. A. Kureshov, A. A. Padalitsa, A. A. Marmalyuk, and R. K. Akchurin, Mod. Electron. Mater. **2**, 45 (2016).

[29] G. Miceli and A. Pasquarello, Phys. Rev. B **93**, 165207 (2016).

[30] B. Saha, J. A. Perez-Taborda, J. H. Bahk, Y. R. Koh, A. Shakouri, M. Martin-Gonzalez, and T. D. Sands, Phys. Rev. B **97**, 085301 (2018).

[31] P. V. Burmistrova, J. Maassen, T. Favaloro, B. Saha, S. Salamat, Y. Rui Koh, M. S. Lundstrom, A. Shakouri, and T. D. Sands, J. Appl. Phys. **113**, 153704 (2013).

[32] M. A. Moram, M. J. Kappers, T. B. Joyce, P. R. Chalker, Z. H. Barber, and C. J. Humphreys, J. Cryst. Growth **308**, 302 (2007).

[33] B. Saha, S. Saber, G. V Naik, A. Boltasseva, E. A. Stach, E. P. Kvam, and T. D. Sands, Phys. Status Solidi **252**, 251 (2015).

[34] B. Saha, J. Acharya, T. D. Sands, and U. V. Waghmare, J. Appl. Phys. **107**, 033715 (2010).

[35] Y. Kumagai, N. Tsunoda, and F. Oba, Phys. Rev. Appl. **9**, 34019 (2018).

[36] N. Tureson, M. Marteau, T. Cabioch, N. Van Nong, J. Jensen, J. Lu, G. Greczynski, D. Fournier, N. Singh, A. Soni, L. Belliard, P. Eklund, and A. le Febvrier, Phys. Rev. B **98**, 205307 (2018).

[37] B. Saha, M. Garbrecht, J. A. Perez-Taborda, M. H. Fawey, Y. R. Koh, A. Shakouri, M. Martin-Gonzalez, L. Hultman, and T. D. Sands, Appl. Phys. Lett. **110**, 252104 (2017).

[38] See Supplemental Material at http://link.aps.org/supplemental/10.1103/PhysRevB.99.161117 for details about growth; structure, microscopic and spectroscopic characterization, electron energy loss spectroscopy, XPS core level spectrum, electronic structure of ScN with V_N, effect of stress on ScN's electronic DOS, and other details.

[39] P. Giannozzi, S. Baroni, N. Bonini, M. Calandra, R. Car, C. Cavazzoni, D. Ceresoli, G. L. Chiarotti, M. Cococcioni, I. Dabo, and others, J. Phys. Condens. Matter **21**, 395502 (2009).

[40] D. Vanderbilt, Phys. Rev. B **41**, 7892 (1990).

[41] V. I. Anisimov, J. Zaanen, and O. K. Andersen, Phys. Rev. B **44**, 943 (1991).

[42] H. J. Monkhorst and J. D. Pack, Phys. Rev. B **13**, 5188 (1976).

[43] J. D. Head and M. C. Zerner, Chem. Phys. Lett. **122**, 264 (1985).

[44] U. Haeussermann, M. Boström, P. Viklund, Ö. Rapp, and T. Björnängen, J. Solid State Chem. **165**, 94 (2002).

[45] S. Kerdsongpanya, B. Alling, and P. Eklund, Phys. Rev. B **86**, 195140 (2012).

[46] D. M. Phase, M. Gupta, S. Potdar, L. Behera, R. Sah, and A. Gupta, AIP Conf. Proc. **1591**, 685 (2014).

[47] A. K. Yadav, S. M. Haque, D. Shukla, R. J. Choudhary, S. N. Jha, and D. Bhattacharyya, AIP Adv. **5**, 117138 (2015).

[48] J. J. Rehr, J. J. Kas, F. D. Vila, M. P. Prange, and K. Jorissen, Phys. Chem. Chem. Phys. **12**, 5503 (2010).

[49] F. M. F. de Groot, Z. W. Hu, M. F. Lopez, G. Kaindl, F. Guillot, and M. Tronc, J. Chem. Phys. **101**, 6570 (1994).

[50] M. Raekers, K. Kuepper, S. Bartkowski, M. Prinz, A. V. Postnikov, K. Potzger, S. Zhou, A. Arulraj, N. Stüßer, R. Uecker, W. L. Yang, and M. Neumann, Phys. Rev. B **79**, 125114 (2009).

[51] M. Räkers, Ph.D. Thesis, University of Osnabrück, 2009.

[52] G. Friedbacher and H. Bubert, *Surface and Thin Film Analysis: A Compendium of Principles, Instrumentation, and Applications* (Wiley, New York, 2011).

[53] S. Pan, X. Liu, M. Guo, S. Fung Yu, H. Huang, H. Fan, and G. Li, J. Mater. Chem. A **3**, 11437 (2015).

[54] S. Chandramohan, J. H. Kang, Y. S. Katharria, N. Han, Y. S. Beak, K. B. Ko, J. B. Park, B. D. Ryu, H. K. Kim, E.-K. Suh *et al.*, J. Phys. D. Appl. Phys. **45**, 145101 (2012).

[55] Q. Wang, X. Liu, M. G. Kibria, S. Zhao, H. P. T. Nguyen, K. H. Li, Z. Mi, T. Gonzalez, and M. P. Andrews, Nanoscale **6**, 9970 (2014).

[56] H. A. Al-Brithen, A. R. Smith, and D. Gall, Phys. Rev. B **70**, 045303 (2004).

[57] L. Lymperakis, P. H. Weidlich, H. Eisele, M. Schnedler, J. Nys, and B. Grandidier, Appl. Phys. Lett. **103**, 152101 (2013).

[58] R. E. Jones, K. M. Yu, S. X. Li, W. Walukiewicz, J. W. Ager, E. E. Haller, H. Lu, and W. J. Schaff, Phys. Rev. Lett. **96**, 125505 (2006).

[59] A. Febvrier, N. Tureson, N. Stilkerich, G. Greczynski, and P. Eklund, J. Phys. D. Appl. Phys. **52**, 035302 (2019).

[60] F. Khairallah and A. Glisenti, Surf. Sci. Spectra **13**, 58 (2006).

[61] P. Cakir, R. Eloirdi, F. Huber, R. J. M. Konings, and T. Gouder, J. Phys. Chem. C **118**, 24497 (2014).

[62] C. Liu, E. F. Chor, L. S. Tan, and Y. Dong, Phys. Status Solidi C **4**, 2330 (2007).

[63] V. V Afanas'ev, S. Shamuilia, M. Badylevich, A. Stesmans, L. F. Edge, W. Tian, D. G. Schlom, J. M. J. Lopes, M. Roeckerath, and J. Schubert, Microelectron. Eng. **84**, 2278 (2007).

[64] G. K. H. Madsen and D. J. Singh, Comput. Phys. Commun. **175**, 67 (2006).